

Well Posed, Stable and Weakly Coupled Fluid Structure Interaction Problems

Jan Nordström* and Sofia Eriksson†

April 26, 2009

Abstract

We investigate problems of fluid structure interaction type and aim for a formulation that leads to a well posed problem and a stable numerical procedure. Our first objective is to investigate if the generally accepted formulations of the FSI problems are the only possible ones.

Our second objective is to derive a numerical coupling which is truly stable. To accomplish that we will use a weak coupling procedure and employ summation-by-parts operators and penalty terms. We compare the weak coupling with other common procedures. We also study the effect of high order accurate schemes.

In multiple dimensions this is a formidable task and for that reason we start by investigating the simplest possible model problem available. As a flow model we use the linearized Euler equations in one dimension and as the structure model we consider a spring.

1 Introduction

Fluid structure interaction (FSI) problems occur in many different areas including for example aerodynamics ([1],[3],[6]), acoustics ([2],[5],[20]) and medicine ([7],[10],[12]). The specific FSI phenomenon called aerodynamic flutter is very dangerous and can cause accidents. It deserves attention in its own right, but it is also an example of a problem where most of the activity is due to the interaction between two separate physical problems.

Unless the coupling between these two problems is well posed and stable, either unphysical growth or damping can occur. (Some formulations try to avoid or decrease the coupling problem, see for example [8]). The unphysical growth could result in expensive counter measures while the unphysical damping can provide a false sense of safety. We will investigate well-posedness and stability in detail and due to the complexity, we will start in one dimension and focus on the spatial problem.

*Department of Information Technology, Scientific Computing, Uppsala University, SE-751 05 Uppsala, Sweden and Department of Computational Physics, FOI, The Swedish Defence Research Agency, SE-164 90 Stockholm, Sweden, Corresponding author, *Email adress:* Jan.Nordstrom@foi.se

†Department of Information Technology, Scientific Computing, Uppsala University, SE-751 05 Uppsala, Sweden

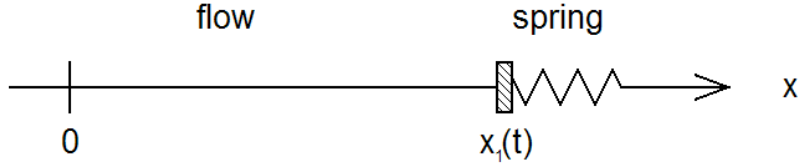


Figure 1: A one-dimensional flow problem interacting with a spring.

First we investigate if the generally accepted formulation of the FSI problem is the only possible one (uniqueness) and such that it does not generate artificial energy growth. In short we will make sure that the coupling is well posed (see [9] for various concepts of well-posedness). Next, given that the problem is well posed, we will make sure that the numerical approximation is accurate and stable. We will study both the linear and non-linear problem.

The rest of the paper proceeds as follows. In section 2 we formulate the problem mathematically. Section 3 deals with the linear problem and well-posedness while the non-linear problem is discussed in section 4. In section 5 we construct stable approximations for the linear semi-discrete approximation and describe the non-linear approximation. Section 6 present the numerical experiments and we draw conclusions in section 7.

2 Mathematical formulation

Our model problem is schematically depicted in Figure 1. The flow part to the left of $x_1(t)$ influence the structural part to the right and vice versa. The governing equations for the flow problem are the symmetric and linearized Euler equations in one dimension

$$U_t + AU_x = 0, \quad 0 \leq x \leq x_1(t) \quad (1)$$

where

$$A = \begin{bmatrix} \bar{u} & \bar{c}/\sqrt{\gamma} & 0 \\ \bar{c}/\sqrt{\gamma} & \bar{u} & \bar{c}\sqrt{\frac{\gamma-1}{\gamma}} \\ 0 & \bar{c}\sqrt{\frac{\gamma-1}{\gamma}} & \bar{u} \end{bmatrix}, \quad U = \begin{bmatrix} \bar{c}^2 \rho / \sqrt{\gamma} \\ \bar{c} \bar{\rho} u \\ \bar{\rho} T / \sqrt{\gamma(\gamma-1)} M_\infty^4 \end{bmatrix}. \quad (2)$$

In (2), ρ , u and T represents the perturbation from the mean value of the density ($\bar{\rho}$), velocity (\bar{u}) and temperature (\bar{T}) respectively, see [15] for more details.

To simplify the analysis we transform equation (1) to a fixed domain using $\xi = x/x_1$ and $\tau = t$. We get

$$x_1(\tau)U_\tau + (A - \xi \dot{x}_1)U_\xi = 0 \quad 0 \leq \xi \leq 1. \quad (3)$$

The structural model, the spring equation is given by

$$m\ddot{\Delta x} + b\dot{\Delta x} + k\Delta x = F_2(U) \quad (4)$$

where $\Delta x = x_1(t) - x_E$, $x_E = 1$ being the equilibrium position of the spring. $m > 0$ is the mass of the "surface" of the spring, $b \geq 0$ is the damping friction coefficient and

$k > 0$ is the spring constant. $F_2(U)$ is the net external force imposed by the flow. Let $V = [V_1 V_2]^T = [\Delta x \ \dot{x}_1]^T$ and rewrite (4) on first order system form as

$$MV_t + KV = F(U) \quad (5)$$

where

$$M = \begin{bmatrix} k & 0 \\ 0 & m \end{bmatrix}, \quad K = \begin{bmatrix} 0 & -k \\ k & b \end{bmatrix}, \quad F = \begin{bmatrix} 0 \\ F_2 \end{bmatrix}. \quad (6)$$

Equation (5) governs the structural part of the FSI problem.

Equations (3) and (5) must be coupled in order to describe the FSI problem correctly. One of the coupling terms is the forcing function $F(U)$ in (5). The other is the boundary condition for the flow equation (3) at $\xi = 1$ which we formulate as

$$B(U) = G(V). \quad (7)$$

The complete coupled non-linear problem in terms of the dependent variables U and V (and changing notation from τ to t) are

$$\begin{aligned} (1 + V_1)U_t + (A - \xi V_2)U_\xi &= 0, & 0 \leq \xi \leq 1, \\ MV_t + KV &= F(U), & \xi = 1 \\ B(U) &= G(V). & \xi = 1 \end{aligned} \quad (8)$$

The problem (8) describes the coupling problem with the unknown forcing function $F(U)$ and coupling condition $B(U) = G(V)$. Boundary conditions at the left boundary and initial conditions must also be supplied. The linearized version of (8) is obtained by letting $V_1 = V_2 = 0$ in the first equation.

We will consider both the linear and non-linear version of (8). The two versions differ at the right boundary where the coupling occurs but require the same treatment at the left boundary.

2.1 Well posed problems

We will use the energy method as our main analysis tool and derive an equation for the energy-rate. We will give well posed boundary conditions at the left boundary but really focus on the interface coupling at the right boundary. At that boundary no external data is provided and for that reason, the following definition for well-posedness is appropriate.

Definition 1. The continuous problem (8) with homogeneous boundary conditions at the left boundary is well posed if the correct number of boundary and coupling conditions are used and

$$\|W\|_t^2 \leq 0, \quad (9)$$

where $W = (U, V)^T$. The equality sign is valid only if the damping in the structure problem is zero ($b = 0$). Time integration of (9) leads to an estimate in terms of initial data.

Remark 2.1. The inequality (9) implies that the spatial operator in (8) is semi-bounded, see [9] for a discussion on semi-boundedness.

2.2 Well posed boundary condition at the left boundary

We use the energy method on the linear version of the first equation in (8) to arrive at the estimate

$$\|U\|_t^2 = -U^T AU|_0^1 = -\left(\bar{c}\frac{(u\bar{\rho}\bar{c} + p)^2}{2} - \bar{c}\frac{(u\bar{\rho}\bar{c} - p)^2}{2}\right)|_0^1 = -2\bar{c}^2\bar{\rho}up|_0^1. \quad (10)$$

We have used $\|U\|^2 = \int_0^1 U^T U d\xi$, $\bar{u} = 0$ (zero mean flow) and $p = \bar{c}^2\rho/\gamma + \bar{\rho}T/(\gamma M_\infty^2)$. Consider the left boundary at $\xi = 0$. In general, a set of well posed boundary conditions are obtained by specifying the ingoing characteristic variable as a function of the outgoing variables and data on the boundary. In this case we use

$$(u\bar{\rho}\bar{c} + p) = \alpha(u\bar{\rho}\bar{c} - p) + g(t). \quad (11)$$

With $g(t) = 0$ we obtain $U^T AU|_0 = (\alpha^2 - 1)\bar{c}\frac{(u\bar{\rho}\bar{c}-p)^2}{2}|_0$ which implies that $-1 \leq \alpha \leq 1$ to obtain a non-positive contribution in line with Definition 1. The most appealing choices of α is 0, -1 and +1, since that corresponds to giving boundary data to $u\bar{\rho}\bar{c} + p$, u and p respectively.

3 The linear problem and well-posedness

We will derive the coupling conditions at the right boundary for the linear problem in two distinctly different ways and start with the more conventional technique.

3.1 Physical coupling approach at the right boundary

The flow is adjacent to the spring which means that the velocity of the flow is equal to the velocity of the spring, i.e. $u(1, t) = \dot{x}_1$. The external force F from the flow onto the spring is ap_1 , where a is the surface size (for simplicity we use $a = 1$) and p_1 is the pressure at $\xi = 1$. In summary the coupling conditions derived by physical reasoning are

$$u(1, t) = \dot{x}_1, \quad F = p(1, t), \quad (12)$$

To make sure that the conditions in (12) are reasonable we must investigate well-posedness. If we multiply the second equation in (8) by V^T we obtain

$$\|V\|_t^2 = (kV_1^2 + mV_2^2)_t = 2V_2F - 2bV_2^2. \quad (13)$$

A linear combination of the estimates (10) and (13), the coupling (12), and ignoring terms at $\xi = 0$ leads to,

$$\|U\|_t^2 + \delta\|V\|_t^2 = -U^T AU|_1 + \delta(2V_2F - 2bV_2^2) = 2\dot{x}_1p_1(-2\bar{c}^2\bar{\rho} + \delta) - 2\delta b\dot{x}_1^2. \quad (14)$$

With $2\bar{c}^2\bar{\rho} = \delta$ we cancel the indefinite term and arrive at a well posed coupling.

3.2 Mathematical coupling approach at the right boundary

In this section we will replace the specific physical coupling assumption (12) and only assume that the coupling conditions are linear relations, i.e.

$$F(U) = F^T U, \quad F^T = [\alpha_1, \alpha_2, \alpha_3], \quad (15)$$

$$B(U) = B^T U = G(V) = G^T V, \quad B^T = [\beta_1, \beta_2, \beta_3], \quad G^T = [\gamma_1, \gamma_2]. \quad (16)$$

Our objective is to see if we automatically arrive at the correct coupling conditions by demanding well-posedness.

The energy-method applied to the linear version of (8), ignoring terms at $\xi = 0$ and a linear combination of the results lead to

$$\|U\|_t^2 + \delta \|V\|_t^2 = -U^T A U + 2\delta(FV_2 - bV_2^2). \quad (17)$$

The absence of V_1 implies that we can take $\gamma_1 = 0$ and $\gamma_2 = 1$. This means that we can solve for $V_2 = \dot{x}_1$ in terms of U and arrive at

$$\|U\|_t^2 + \delta \|V\|_t^2 = -U^T [A - \delta(BF^T + FB^T)]U - 2\delta b U^T B B^T U. \quad (18)$$

For zero damping ($b = 0$) in the system, the symmetric matrix $[A - \delta(BF^T + FB^T)]$ must vanish for well-posedness. We have the condition

$$\begin{bmatrix} -2\delta\alpha_1\beta_1 & \bar{c}/\sqrt{\gamma} - \delta(\alpha_1\beta_2 + \alpha_2\beta_1) & -\delta(\alpha_1\beta_3 + \alpha_3\beta_1) \\ \bar{c}/\sqrt{\gamma} - \delta(\alpha_1\beta_2 + \alpha_2\beta_1) & -2\delta\alpha_2\beta_2 & \bar{c}\sqrt{\frac{\gamma-1}{\gamma}} - \delta(\alpha_2\beta_3 + \alpha_3\beta_2) \\ -\delta(\alpha_1\beta_3 + \alpha_3\beta_1) & \bar{c}\sqrt{\frac{\gamma-1}{\gamma}} - \delta(\alpha_2\beta_3 + \alpha_3\beta_2) & -2\delta\alpha_3\beta_3 \end{bmatrix} = 0.$$

By inspection we find that the boundary matrix $[A - \delta(BF^T + FB^T)]$ vanish for

$$\alpha_2 = \beta_1 = \beta_3 = 0, \quad \alpha_1 = \frac{1}{\delta\beta_2} \frac{\bar{c}}{\sqrt{\gamma}}, \quad \alpha_3 = \frac{1}{\delta\beta_2} \bar{c} \sqrt{\frac{\gamma-1}{\gamma}} \quad (19)$$

or

$$\beta_2 = \alpha_1 = \alpha_3 = 0, \quad \beta_1 = \frac{1}{\delta\alpha_2} \frac{\bar{c}}{\sqrt{\gamma}}, \quad \beta_3 = \frac{1}{\delta\alpha_2} \bar{c} \sqrt{\frac{\gamma-1}{\gamma}}. \quad (20)$$

The relations in (19) and (20) lead to the following two alternative forms of coupling conditions

$$\dot{x}_1 = (\beta_2 \sqrt{2\bar{\rho}\bar{c}})u, \quad F = \left(\frac{\sqrt{2\bar{c}}}{\delta\beta_2}\right)p \quad \text{or} \quad \dot{x}_1 = (\alpha_2 \sqrt{2\bar{\rho}\bar{c}})p, \quad F = \left(\frac{\sqrt{2\bar{c}}}{\delta\alpha_2}\right)u. \quad (21)$$

The two relations in (21) are obtained without any physical knowledge at all.

To sort out the correct formulation we must add the requirement that the fluid is adjacent to the spring i.e. $u = \dot{x}_1$. That condition removes the second set of conditions in (20) and leads to the scaling $\beta_2 = 1/(\sqrt{2\bar{\rho}\bar{c}})$. The choice $\delta = 2\bar{\rho}\bar{c}^2$ yield $F = p$. We summarize the result so far for the linear problem (8) in the following theorem.

Theorem 3.1. *The linearized version of (8) (obtained by letting $V_1 = V_2 = 0$ in the first equation) combined with the boundary condition (11) and the coupling condition (12) is well posed in the sense of Definition 1.*

Remark 3.2. To arrive at the correct coupling conditions (12) by only demanding well-posedness was not possible. That lead to two possible versions of coupling conditions in (20). The physical condition $u = \dot{x}_1$ (which can be seen as an accuracy requirement) had to be imposed in order to sort out the correct version.

3.3 The continuous spectrum

In the linear setting with $\bar{u} = 0$ the system (1) have one zero eigenvalue and we can reduce our problem to a 2×2 -system where ρ and T are linearly dependent. We get $\bar{c}^2(\gamma - 1)M_\infty^2\rho - \bar{\rho}T = \text{constant}$. To simplify further we will keep a linear combination of them, namely the pressure p . We get the reduced system

$$W_t + \begin{pmatrix} 0 & \bar{c} \\ \bar{c} & 0 \end{pmatrix} W_x = 0, \quad W = \begin{pmatrix} u\bar{\rho}\bar{c} \\ p \end{pmatrix}, \quad (22)$$

which on diagonal form becomes

$$w_t + \Lambda w_x = 0, \quad w = \frac{1}{\sqrt{2}} \begin{bmatrix} u\bar{\rho}\bar{c} - p \\ u\bar{\rho}\bar{c} + p \end{bmatrix}, \quad \Lambda = \begin{bmatrix} -\bar{c} & 0 \\ 0 & \bar{c} \end{bmatrix}. \quad (23)$$

By Laplace transforming (23) we obtain $s\hat{w} + \Lambda\hat{w}_x = 0$. The Ansatz: $\hat{w} = \Psi e^{\lambda x}$ leads to $(sI + \lambda\Lambda)\Psi = 0$. A non-trivial solution yields $\lambda_{1,2} = \pm s/\bar{c}$, $\Psi_1 = [1 \ 0]^T$, $\Psi_2 = [0 \ 1]^T$ and finally

$$\hat{w} = \sigma_1 \Psi_1 e^{\lambda_1 x} + \sigma_2 \Psi_2 e^{\lambda_2 x} = (\sigma_1 e^{+sx/\bar{c}}, \sigma_2 e^{-sx/\bar{c}})^T. \quad (24)$$

The coefficients σ_1 and σ_2 will be determined by the boundary conditions.

At the left boundary we consider the boundary condition (11) with $\alpha = +1, -1, 0$ respectively. That leads to

$$\sqrt{2}\hat{p}|_0 = \hat{w}_2|_0 - \hat{w}_1|_0 = \sigma_2 - \sigma_1 = \hat{g}_1 \quad (25)$$

$$\sqrt{2}\bar{\rho}\bar{c}\hat{u}|_0 = \hat{w}_2|_0 + \hat{w}_1|_0 = \sigma_2 + \sigma_1 = \hat{g}_2 \quad (26)$$

$$(\bar{\rho}\bar{c}\hat{u}|_0 + \hat{p}|_0)/\sqrt{2} = \hat{w}_2|_0 = \sigma_2 = \hat{g}_3 \quad (27)$$

At the right boundary we specify the velocity (required for well-posedness), hence

$$\sqrt{2}\bar{\rho}\bar{c}\hat{u}|_1 = \hat{w}_2|_1 + \hat{w}_1|_1 = \sigma_2 e^{-s/\bar{c}} + \sigma_1 e^{s/\bar{c}} = \hat{g}_4 = \sqrt{2}\bar{\rho}\bar{c}\hat{V}_2 \quad (28)$$

The data g_4 is obtained from the the structural part which we consider next.

The Laplace transform of (5) yields

$$s\hat{V} + \begin{bmatrix} 0 & -1 \\ k/m & b/m \end{bmatrix} \hat{V} = \begin{bmatrix} 0 \\ \hat{p}|_1/m \end{bmatrix} \Rightarrow \hat{V} = \frac{\hat{p}|_1}{ms^2 + bs + k} \begin{bmatrix} 1 \\ s \end{bmatrix}. \quad (29)$$

The boundary conditions (28) now yields

$$\frac{s(\hat{w}_2|_1 - \hat{w}_1|_1)}{\sqrt{2}(ms^2 + bs + k)} = \frac{\hat{w}_2|_1 + \hat{w}_1|_1}{\sqrt{2}\bar{\rho}\bar{c}} \Rightarrow \hat{w}_1|_1(1 + \varphi) + \hat{w}_2|_1(1 - \varphi) = 0, \quad (30)$$

where $\varphi(s) = \bar{\rho}cs/(ms^2 + bs + k)$ and $\hat{w}_1|_1 = \sigma_1 e^{s/\bar{c}}$ and $\hat{w}_2|_1 = \sigma_2 e^{-s/\bar{c}}$.

The linear equations system for determining the coefficients σ_1 and σ_2 can formally be written

$$C(s)\sigma = \hat{g} \quad (31)$$

where

$$C(s) = \begin{bmatrix} -\alpha & 1 \\ (1 + \varphi)e^{s/\bar{c}} & (1 - \varphi)e^{-s/\bar{c}} \end{bmatrix}, \quad \sigma = \begin{bmatrix} \sigma_1 \\ \sigma_2 \end{bmatrix}, \quad g = \begin{bmatrix} \hat{g}_i \\ 0 \end{bmatrix}. \quad (32)$$

A unique solution is obtained for

$$|C(s)| = -(e^{s/\bar{c}}(1 + \varphi) + e^{-s/\bar{c}}\alpha(1 - \varphi)) \neq 0. \quad (33)$$

The s values that lead to a singular matrix $C(s)$ us the gives the spectrum or the eigenvalues of the problem. The value of $\alpha = 1$ corresponds to giving data to p , $\alpha = -1$ to u and $\alpha = 0$ to $\bar{\rho}\bar{c}u + p$. If the damping of the system is zero ($b = 0$) and data is given to either u or p , then all eigenvalues will be on the imaginary axis. Each eigenvalue will correspond to an eigenfrequency of the coupled system.

4 The non-linear problem and well-posedness

The full non-linear representation of the flow system is given by (3) or equivalently the first equation in (8) . The energy method gives

$$((1 + V_1)\|U\|^2)_t = -U_1^T (A - V_2 I_3) U_1 + U_0^T A U_0. \quad (34)$$

In comparison with the linear case, the norm is slightly modified and at the interface between the fluid and the spring, an additional term $V_2 U^T U|_1$ is added on. The conditions at the left boundary is the same as in the linear case. The term $V_2 U^T U|_1$ is indefinite since V_2 changes sign. This means that the non-linear problem is not well-posed in the sense of Definition 1. We summarize this as follows.

Theorem 4.1. *The non-linear problem (8) combined with the boundary condition (11) and the coupling condition (12) is not well posed in the sense of Definition 1.*

5 The semi-discrete approximation and stability

We will do numerical calculations using the both the linear and non-linear equations. For both cases we will use the linear coupling treatment developed above. With a slight abuse of notation we use U, V both for the continuous and discrete vectors.

5.1 The semi-discrete linear formulation

The discrete version of the linearized flow equation in (8) with the boundary and interface conditions (11), (12) imposed as penalty terms is written as

$$U_t + (P^{-1}Q \otimes A)U = (P^{-1}E_N \otimes \Sigma)(U - g) + (P^{-1}E_0 \otimes \Pi)(U - r). \quad (35)$$

In (35) we have used the summation-by-parts (SBP) difference operator $P^{-1}Q$ (see [11],[19]) and imposed the boundary conditions using the SAT technique [4]. The SBP difference operators satisfy the relations

$$P = P^T > 0, \quad Q + Q^T = E_N - E_0 = \text{diag}(-1, 0, \dots, 0, 1), \quad (36)$$

and hence they mimic integration by parts perfectly. More details on the weak imposition of boundary and interface conditions using the SAT technique will be given below. For a read-up on this technique see [4],[14],[17],[18].

By multiplying (35) with $U^T(P \otimes I_3)$ from the left, adding the transpose and using the relation (36) we obtain

$$\frac{d}{dt} \|U\|_{\bar{P}}^2 + U^T((-E_0 + E_N) \otimes A)U = 2U_N^T \Sigma(U_N - g_N) + 2U_0^T \Pi(U_0 - r_0). \quad (37)$$

For convenience we have introduced the notation $\bar{P} = P \otimes I_3$. By adding the estimate for the structure part using the same scaling δ as in the continuous case we find

$$\begin{aligned} \frac{d}{dt} (\|U\|_{\bar{P}}^2 + \delta \|V\|^2) &= U_0^T A U_0 + 2U_0^T \Pi(U_0 - r_0) \\ &\quad - U_N^T A U_N + 2U_N^T \Sigma(U_N - g_N) + 2\delta F V_2 - 2\delta b V_2^2. \end{aligned} \quad (38)$$

5.2 The semi-discrete non-linear formulation

In the non-linear discrete case we have an additional matrix operator Ξ which models the impact of the coordinate ξ . Since the matrices Q and Ξ do not commute we must split the derivative terms in a symmetric and skew-symmetric part, see [16] for more details. Consider the first equation in (8). We split the term as

$$\xi U_\xi = (\xi U_\xi)/2 + ((\xi U)_\xi - U)/2, \quad (39)$$

and use the following discrete representations

$$A U_\xi \sim (P^{-1}Q \otimes A)U, \quad \xi U_\xi \sim (\Xi P^{-1}Q \otimes I_3)U, \quad (\xi U)_\xi \sim (P^{-1}Q \Xi \otimes I_3)U.$$

We have used $\xi \sim \Xi = \text{diag}(0 \ 1/N \ 2/N \ \dots \ 1)$. The semi-discrete version of the non-linear flow equation in (8) is written as

$$\begin{aligned} (1 + V_1)U_t &+ (P^{-1}Q \otimes A)U - V_2 ((\Xi P^{-1}Q \otimes I_3) + (P^{-1}Q \Xi \otimes I_3) - (I_N \otimes I_3)) U/2 \\ &= (P^{-1}E_N \otimes \Sigma)(U - g) + (P^{-1}E_0 \otimes \Pi)(U - r). \end{aligned} \quad (40)$$

The energy rate is given by multiplying (40) from the left by $U^T(P \otimes I_3)$, adding the transpose, using (36), adding the spring estimate and observing that $(1 + V_1)_t = V_2$. We have

$$\begin{aligned} ((1 + V_1)\|U\|_{\bar{P}}^2 + \delta \|V\|^2)_t &= U_0^T A U_0 + 2U_0^T \Pi(U_0 - r_0) \\ &\quad - U_N^T (A - V_2 I_3) U_N + 2U_N^T \Sigma(U_N - g_N) + 2\delta F V_2 - 2\delta b V_2^2. \end{aligned} \quad (41)$$

The difference between the linear (38) and non-linear (41) estimates is the form of the norm and the additional term $V_2 U_N^T U_N$ (the same difference as in the continuous case). To get stability in the linear case we must choose the penalty matrices Σ and Π in a specific way.

5.3 A stable left boundary procedure

Consider the boundary terms at $\xi = 0$ and boundary condition $u(0, t) = r(t)$. By assuming that $r = 0$ we obtain,

$$U^T AU + 2U^T \Pi U = 2\bar{\rho}\bar{c}^2 u p + 2U^T \begin{bmatrix} 0 & \pi_{12} & 0 \\ 0 & \pi_{22} & 0 \\ 0 & \pi_{32} & 0 \end{bmatrix} U = 2\bar{\rho}\bar{c}u p(\bar{c} + \pi_2) + 2\pi_{22}(\bar{\rho}\bar{c}u)^2. \quad (42)$$

where we have substituted $\pi_{12} = \pi_2/\sqrt{\gamma}$, $\pi_{32} = \pi_2\sqrt{(\gamma-1)}/\gamma$ and omitted the grid index 0 on all variables. The specific form of Π is due to the fact that the penalty should just manipulate u which sits in the second component of U . By choosing $\pi_2 = -\bar{c}$ and $\pi_{22} \leq 0$ we get a stable left boundary treatment.

The cases where $p(0, t) = r(t)$ or $\bar{\rho}\bar{c}u(0, t) + p(0, t) = r(t)$ are used as boundary conditions is treated similarly, and we end up with the following three penalty matrices,

$$\Pi_u = \begin{bmatrix} 0 & -\bar{c}/\sqrt{\gamma} & 0 \\ 0 & \pi & 0 \\ 0 & -\bar{c}\sqrt{\frac{\gamma-1}{\gamma}} & 0 \end{bmatrix}, \quad \Pi_p = \begin{bmatrix} \pi/\gamma & 0 & \pi\frac{\sqrt{\gamma-1}}{\gamma} \\ -\bar{c}/\sqrt{\gamma} & 0 & -\bar{c}\sqrt{\frac{\gamma-1}{\gamma}} \\ \pi\frac{\sqrt{\gamma-1}}{\gamma} & 0 & \pi\frac{\gamma-1}{\gamma} \end{bmatrix}, \quad \pi \leq 0 \quad (43)$$

$$\Pi_{\bar{\rho}\bar{c}u+p} = \begin{bmatrix} \pi/\gamma & \pi/\sqrt{\gamma} & \pi\frac{\sqrt{\gamma-1}}{\gamma} \\ \pi/\sqrt{\gamma} & \pi & \pi\sqrt{\frac{\gamma-1}{\gamma}} \\ \pi\frac{\sqrt{\gamma-1}}{\gamma} & \pi\sqrt{\frac{\gamma-1}{\gamma}} & \pi\frac{\gamma-1}{\gamma} \end{bmatrix}, \quad \pi \leq -\frac{\bar{c}}{4}. \quad (44)$$

In summary, the three penalty matrices in (43) and (44) above with the parameter choices indicated lead to a stable left boundary treatment for both the linear and non-linear case.

5.4 A stable right boundary procedure for the linear case

Consider the coupling terms (CT) at the right boundary where $\xi = 1$,

$$\text{CT} = -U_N^T A U_N + 2U_N^T \Sigma (U_N - g_N) + 2\bar{\rho}\bar{c}^2 F V_2 - 2\bar{\rho}\bar{c}^2 b V_2^2.$$

The coupling conditions $F = p_N$, $g_N = \bar{\rho}\bar{c}V_2$ and zero damping ($b = 0$) leads to

$$\begin{aligned} \text{CT} &= -2\bar{\rho}\bar{c}^2 u_N p_N + 2U_N^T \begin{bmatrix} 0 & \sigma_1 & 0 \\ 0 & \sigma_2 & 0 \\ 0 & \sigma_3 & 0 \end{bmatrix} (U_N - \bar{\rho}\bar{c}V_2) + 2\bar{\rho}\bar{c}^2 p_N V_2 \\ &= 2\bar{\rho}\bar{c}(u_N - V_2)(-\bar{c}p_N + \sigma p_N + \sigma_2 u_N \bar{\rho}\bar{c}). \end{aligned} \quad (45)$$

To simplify we have inserted the relations $\sigma_1 = \sigma/\sqrt{\gamma}$ and $\sigma_3 = \sigma\sqrt{(\gamma-1)}/\gamma$. Clearly, $\sigma = \bar{c}$ and $\sigma_2 = 0$ leads to $\text{CT} = 0$ and a stable boundary treatment for the right boundary. The final form of Σ is

$$\Sigma = \begin{bmatrix} 0 & \bar{c}/\sqrt{\gamma} & 0 \\ 0 & 0 & 0 \\ 0 & \bar{c}\sqrt{\frac{\gamma-1}{\gamma}} & 0 \end{bmatrix}. \quad (46)$$

Remark 5.1. Note the similarity between the matrix elements in the penalty matrices (43),(44),(46) and the matrix elements of A in (2)

5.5 The right boundary procedure in the non-linear case

By applying the exact same procedure (the penalty matrix in (46) with the same data) for the non-linear case we obtain

$$CT = V_2 U_N^T U_N. \quad (47)$$

Clearly this is not stable since the sign of the right-hand-side varies. We will investigate numerically what this means and come back to this issue.

6 Numerical simulations

The semi-discrete FSI problem was integrated in time as a large system of ordinary differential equation of the form $y_t = M(t)y + g(t)$, where $y = [w; v]$ and $g(t)$ includes the boundary data. To integrate the system in time we used the classical 4th order Runge-Kutta method. In the linear case, M is a constant $(3N + 5) \times (3N + 5)$ matrix. In the non-linear case, $M = M(t)$ is slightly modified. The structure of the matrix M depend on the boundary and coupling conditions. For details, see Appendix A. In all the calculations below we have used the parameters $m = 0.1$, $b = 0$, $k = 1$, $\bar{\rho} = \bar{c} = 1$.

6.1 Numerical simulations in the linear case

We start by verifying that our numerical approximation is correct by comparing the numerical eigenvalues (or eigenfrequencies) with the spectrum of the continuous operator. With the damping coefficient of the spring b being zero and specifying the pressure p at the left boundary, the continuous spectra is purely imaginary.

In Figure 2, the eigenvalues of the linear discrete (second order accurate) operator M are shown together with the continuous spectra. The position of the continuous eigenvalues s are marked as dashed lines. The numerical eigenvalues converge to the continuous ones as the number of grid-points N increases (plus additional purely numerical eigenvalues). The eigenvalues are purely imaginary and symmetrically distributed around the real axis. Only the ones with positive imaginary part are shown.

To further check our numerical scheme we gave the spring a small displacement as initial data, used the pressure boundary condition with zero data and recorded the time history of the position $1 + V_1$ of the spring. Fourier transformation gave us the frequency response in figure 3. We used the same parameter values as above and clearly the angular frequencies correspond to the discrete spectra. We also see the convergence of the numerical spectrum to the continuous one.

The calculations so far has been done with the weak penalty implementation of the boundary and interface conditions. In that case we can prove stability by energy estimates as was done in sections 5.3, 5.4 above. This is not the most common way to implement coupling or boundary conditions. Often, so called strong implementation (or injection) is used, see [13].

In the injection method, the values of the boundary conditions and coupling condition are directly given to the appropriate variable. For the coupling procedure it means that the value of the spring velocity V_2 is directly given to the velocity of the

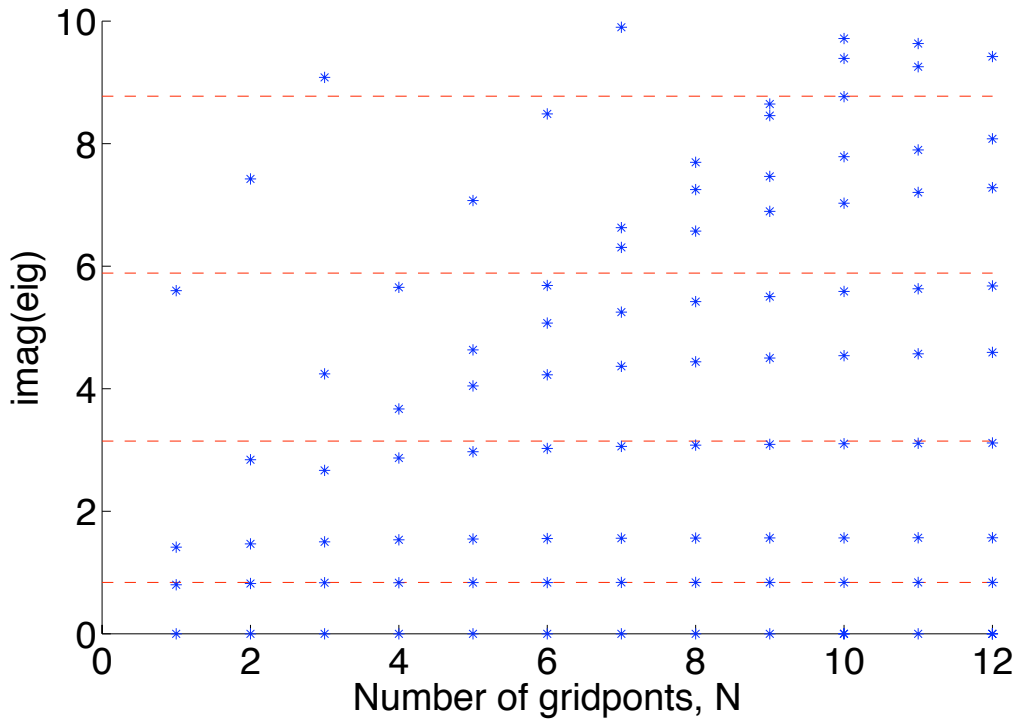


Figure 2: Numerical eigenvalues of the operator M as a function of the number of grid-points. The dashed lines indicate the position of the continuous eigenvalues s .

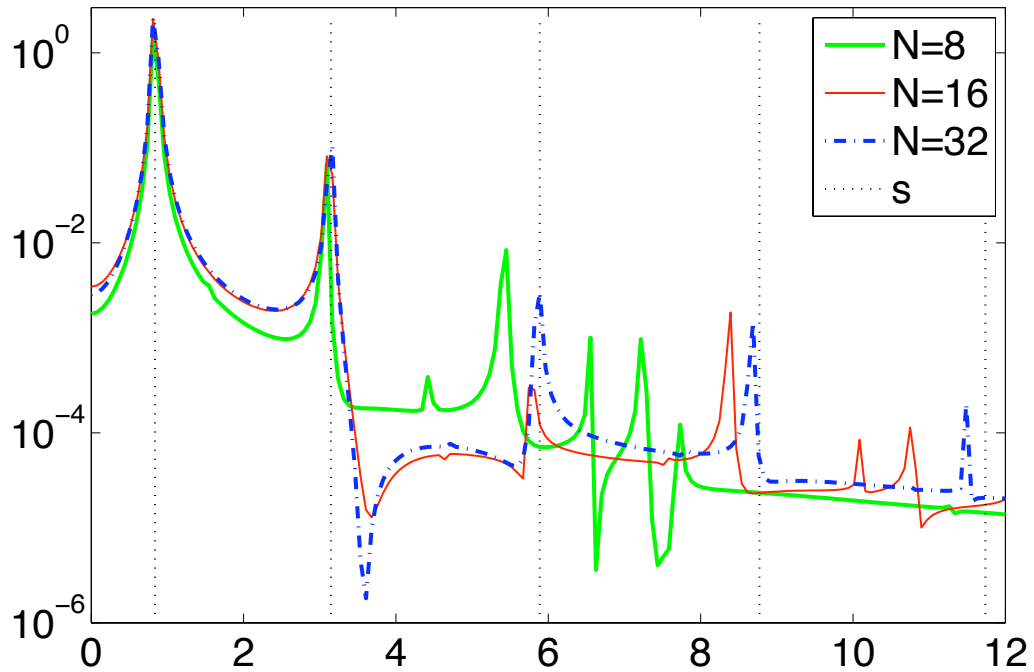


Figure 3: Frequency response for increasing number of gridpoints from an initial small displacement of the spring. The continuous frequencies are indicated by dashed lines.

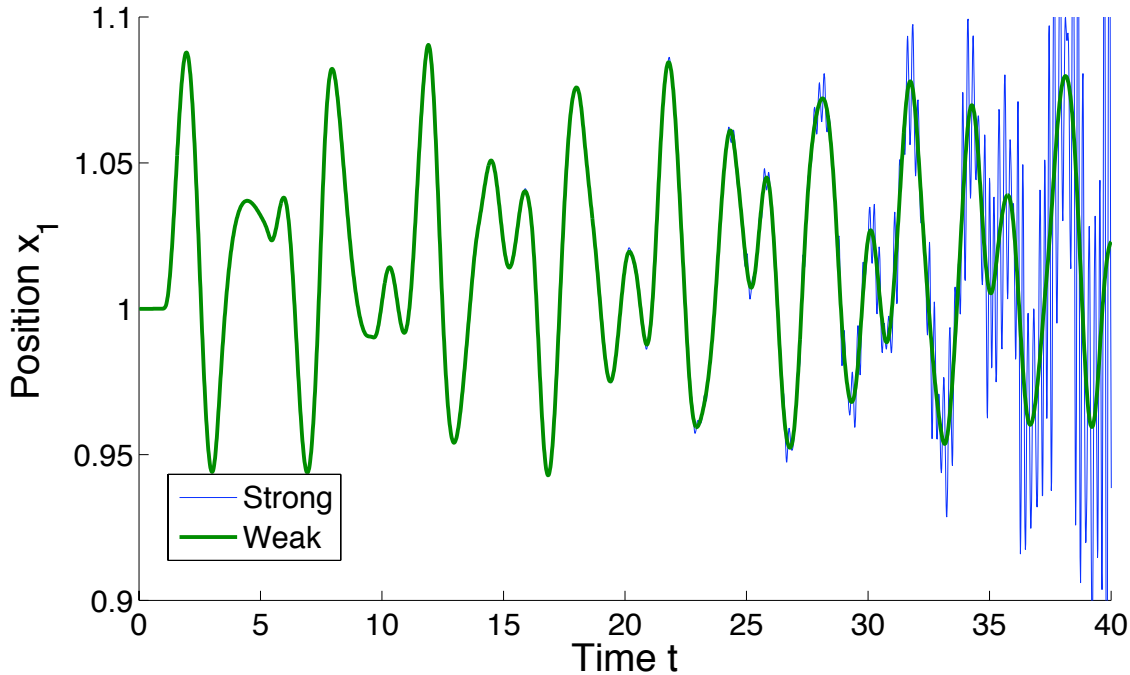


Figure 4: The effect of strong and weak imposition of boundary conditions for $\omega = \pi$. The strong calculation explodes shortly after $t = 40$ while the weak calculation remains stable. Note that π is not an eigenfrequency.

flow problem as $u_n = V_2$. With injection, specific numerical boundary conditions must also be employed (they are pre-computed or integrated in the SBP operator). We have used first and second order extrapolation.

The effect of the strong boundary procedure along with a stable calculation using the weak form with SBP operators can be seen in figure 4. At the left boundary we specify the velocity with an amplitude of 0.1 and the frequency $\omega = \pi$. Note that π is not an eigenfrequency. Clearly the weak treatment with SBP operators is superior. The incorrect boundary treatment for the injection method leads to an instability that resembles and can be mistaken for flutter.

Next we study the effect of higher order schemes. In Figures 5 and 6 we show the difference between second, fourth and sixth order accurate schemes when computing eigenfrequencies. The higher order ones are more accurate and converges faster. In Figure 6 we have only kept the numerical eigenvalues that converge to the real eigenvalues. The purely numerical ones are removed for clarity, cf figure 2 where all the eigenvalues are shown.

High order of accuracy is especially important when dealing with high eigenfrequencies and long time calculations. Figure 7 show that quite different results are obtained using second and fourth order accurate methods. The second order method completely misses the long time growth that is captured by the fourth order accurate method.

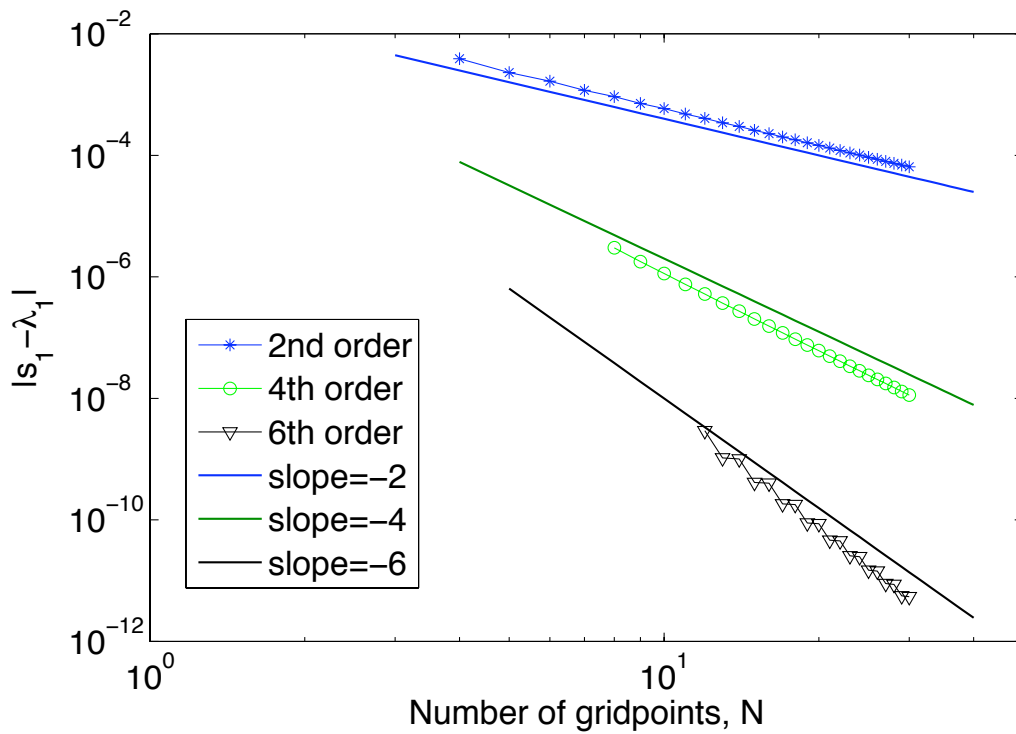


Figure 5: The convergence of the lowest numerical eigenfrequency ($\omega = 0.83756479484021$) for different orders of accuracy. Weak imposition of boundary conditions is used.

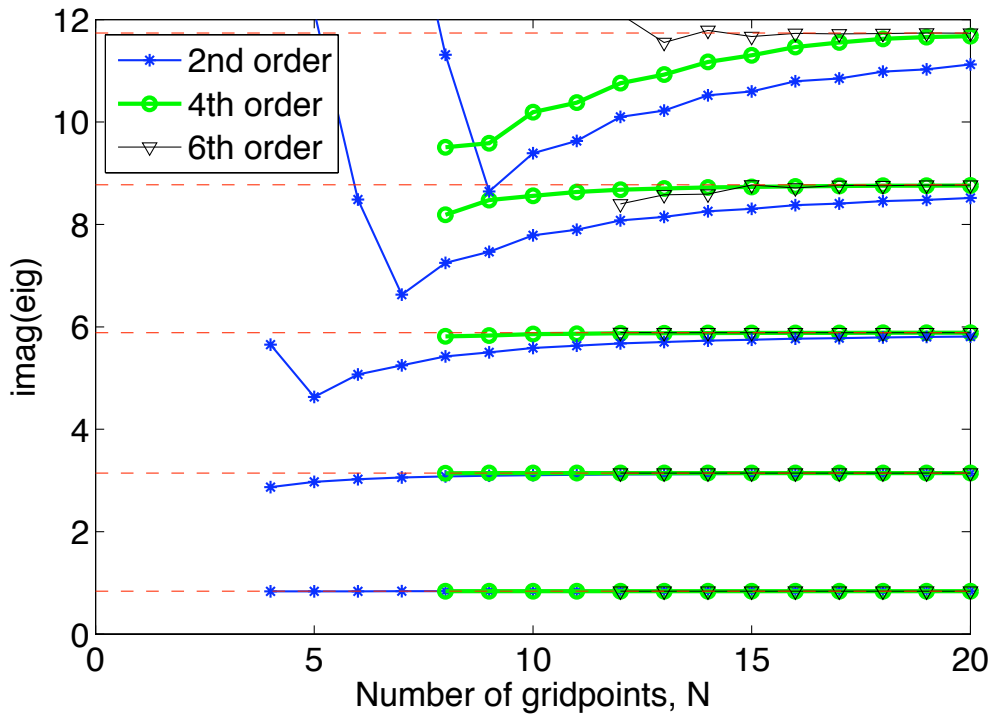


Figure 6: The effect higher order schemes have when computing the five lowest eigenfrequencies. All schemes use weak imposition of boundary conditions.

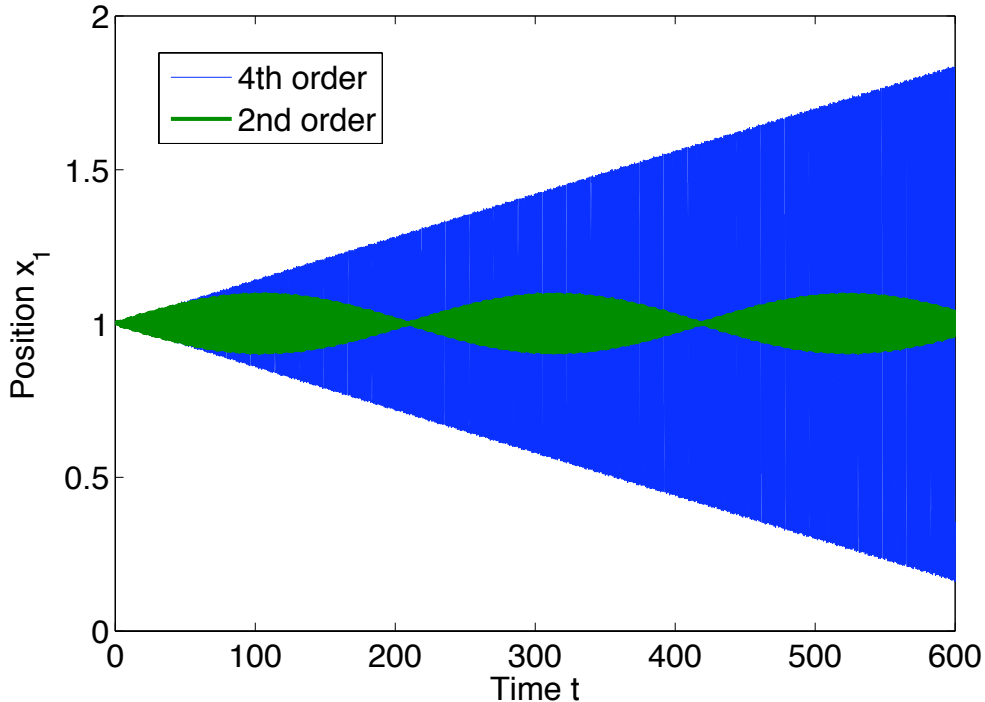


Figure 7: The second order method misses the long time growth of the high frequency mode ($\omega = 5.88659330731852$) that is captured by the fourth order accurate method.

6.2 Numerical simulations in the non-linear case

In this section we return to the difference between the linear and non-linear version of the equations and the approximations. We start by studying the example shown in Figure 8. In these two calculations we have used exactly the same boundary and coupling conditions and we are feeding in the pressure at an eigenfrequency of the linear problem at the left boundary.

As expected the linear problem grows linearly in time. The non-linear problem does not. The difference is mainly due to the remaining source term in (47) which changes sign in an oscillatory manner. Note the higher frequency content in the nonlinear calculation. Another way of looking at the linear and non-linear problem is shown in figures 9 and 10 where the effect of a small and large initial displacement is shown. Clearly, for small amplitudes, the linear theory describes the phenomenon while the non-linear effects dominate for large deformations.

As was shown in section 4, the non-linear right hand side problem is not well posed due to the remaining term $V_2 U^T U$ at $\xi = 1$ on the right-hand-side in the energy estimate. The lack of well-posedness results (of course) in a lack of stability as shown in section 4. This theoretical deficiency does not necessarily lead to an unbounded growth which was exemplified in figures 8 and 10. In fact the growth in the non-linear problem was less than the one in the corresponding linear problem for all the cases we investigated.

One possibility to correct the lack of well-posedness would be to add a boundary

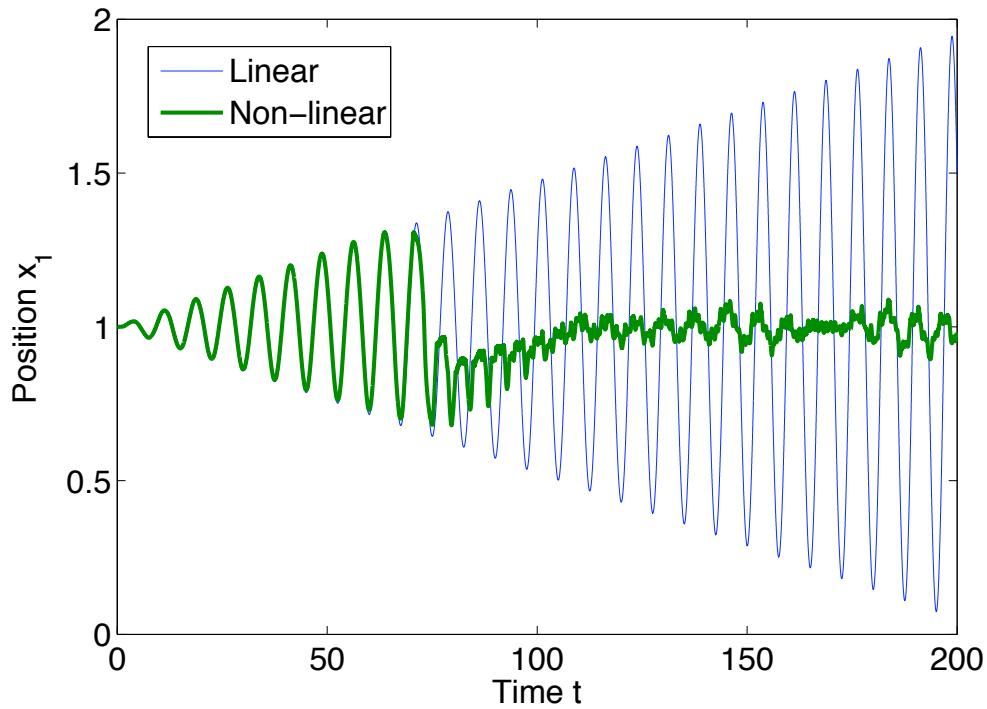


Figure 8: The linear and non-linear response when feeding in pressure variations at the left boundary at an eigenfrequency ($\omega = 0.83756479484021$) of the linear problem.

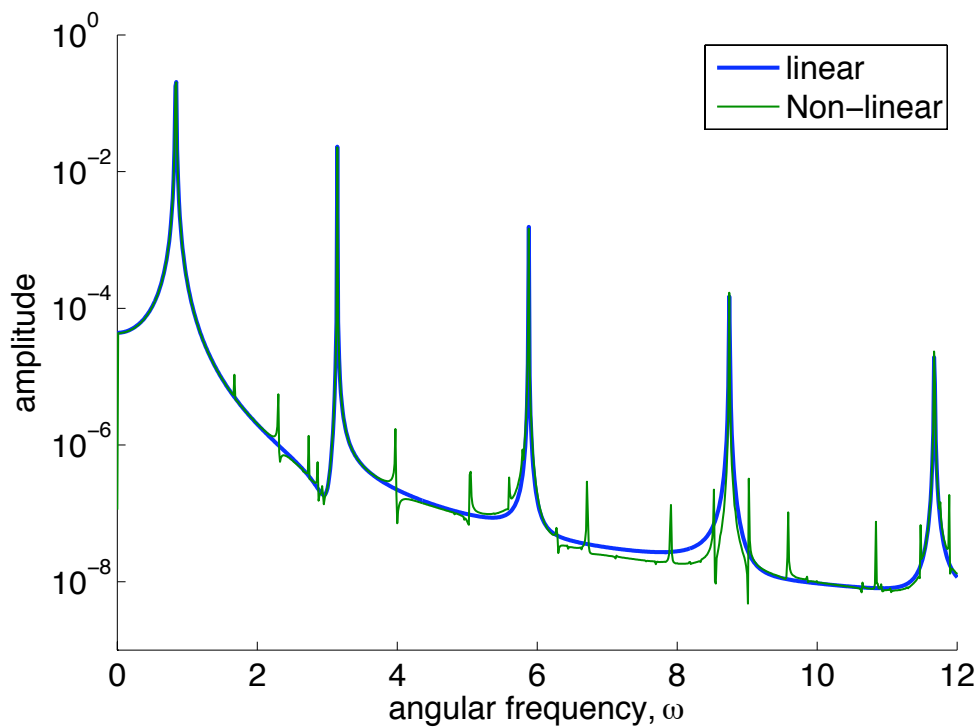


Figure 9: The frequency response for a small initial displacement, $\Delta x = 0.01$.

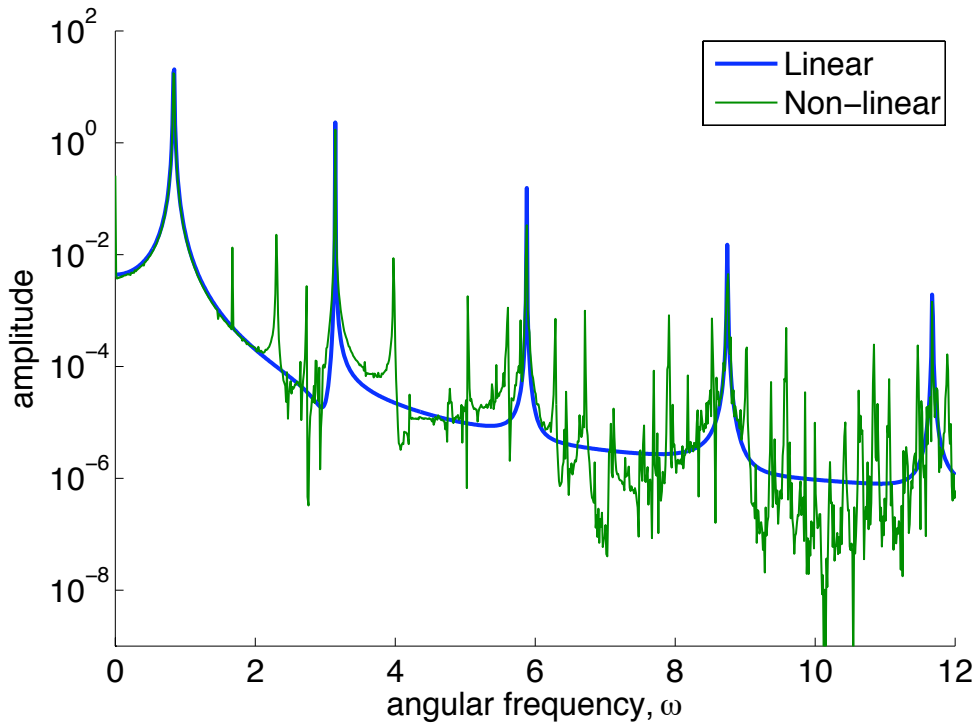


Figure 10: The frequency response for a large initial displacement, $\Delta x = 0.10$.

condition at the right boundary when V_2 is positive. However, it is difficult to find a (non-awkward) boundary condition that remove the growth term. Also, even if that could be done, the data for the boundary condition do not really exist for the Euler case. Another possibility would be to change equation set and use the Navier-Stokes equations which naturally allows for more boundary conditions and types of data.

Our conclusion is that the lack of well-posedness cannot be corrected in a straight forward manner for our problem. The lack of well-posedness and stability for this model problem might exist even for three-dimensional FSI calculations using the Euler equations.

7 Summary and conclusions

We have investigated well-posedness of FSI problems. As a flow model we have used the linearized Euler equations in one dimension and as the structure model, a spring. We have studied both the non-linear and linear problem. The non-linearity stems from large deflections and high speed of the spring.

It was shown that the generally accepted formulation of the the linear FSI problem is the only possible one. It was also shown that coupling in the linear case can be derived using the demand for well-posedness as the main tool. The non-linear version of the problem is not well-posed in the classical sense.

For the linear problem we derived and proved that the numerical coupling using summation-by-parts operators and weak boundary conditions is truly stable. We veri-

fied our numerical procedure by showing that the numerical eigenfrequencies converge to the analytical eigenfrequencies (the spectrum) of the coupled partial differential equations.

We compared our numerical procedure with the common way of using injection to impose the boundary and coupling conditions for the linear problem. Our procedure is stable and gave correct results while the injection procedure lead to instabilities that easily can be interpreted as flutter.

We also studied the effect of higher order schemes. It was shown that the higher order accurate approximations converges faster and more easily capture the effects related to the higher eigenfrequencies.

Non-linear calculations using exactly the same coupling procedures as in the linear case were performed. It was found that the non-linear and linear calculations agree well for small deflections, which verified the non-linear scheme since the linear scheme is provable correct. It was also shown that for large deflections and high speed of the spring, clear differences exist.

The lack of well-posedness (and stability) for the non-linear problem did not lead to an unbounded growth for the cases we studied. In fact, the growth in the non-linear problem was less than the one in the corresponding linear problem for all the cases investigated.

Finally, the comparison between the linear and non-linear problem was discussed and it was concluded that it would be difficult to correct the lack of well-posedness for this problem. It was also noted that the lack of well-posedness and stability for this model problem might very well exist even for realistic three-dimensional FSI calculations using the Euler equations.

A The time integration procedure

We start by constructing the scheme for the linear problem. The non-linear scheme is easily obtained by a few small modifications.

A.1 The linear scheme

We will integrate the coupled system as one large system of ordinary differential equations. The formulation including boundary conditions is

$$U_t = -(P^{-1}Q \otimes A)U + (P^{-1}E_N \otimes \Sigma)(U - g(V)) + (P^{-1}E_0 \otimes \Pi)(U - r) \quad (48)$$

$$V_t = -BV + F(U), \quad (49)$$

where

$$B = M^{-1}K = \begin{bmatrix} 0 & -1 \\ k/m & b/m \end{bmatrix}, \quad F = \begin{bmatrix} 0 \\ p_N/m \end{bmatrix}. \quad (50)$$

By introducing the notation $\tilde{A} = (P^{-1}Q \otimes A)$, $\tilde{\Sigma} = (P^{-1}Q \otimes \Sigma)$ and $\tilde{\Pi} = (P^{-1}Q \otimes \Pi)$ we can rewrite the system as

$$U_t = (-\tilde{A} + \tilde{\Sigma} + \tilde{\Pi})U - \tilde{\Sigma}g - \tilde{\Pi}r \quad (51)$$

$$V_t = -BV + F, \quad (52)$$

where the coupling between (51) and (52) is included in $\tilde{\Sigma}g(V)$ and $F(U)$ as

$$\tilde{\Sigma}g(V) = P_{NN}^{-1}\bar{\rho}\bar{c}^2V_2 \left[0, \dots, 0, 1/\sqrt{\gamma}, 0, \sqrt{(\gamma-1)/\gamma}\right]^T \quad (53)$$

$$F(U) = \left[0, \left(U_{3N+1}/\sqrt{\gamma} + U_{3N+3}\sqrt{(\gamma-1)/\gamma}\right)/m\right]^T. \quad (54)$$

Next we form $y = [U; V]$ as a vector of length $3(N+1) + 2$ where $N+1$ is the number of grid-points. This gives us the final form of the system which is now ready for time integration.

$$y_t = \begin{bmatrix} & & 0 & 0 \\ & & \vdots & \\ -\tilde{A} + \tilde{\Sigma} + \tilde{\Pi} & & \vdots & \kappa_1 \\ & & 0 & \kappa_2 \\ 0 & \dots & 0 & 0 \\ 0 & \dots & 0 & 0 \end{bmatrix} y + \begin{bmatrix} & & 0 & 0 \\ & & \vdots & \vdots \\ 0 & \dots & 0 & -B \\ 0 & \dots & \kappa_3 & 0 \end{bmatrix} y - \begin{bmatrix} \tilde{\Pi}r \\ 0 \\ 0 \end{bmatrix}. \quad (55)$$

The coupling terms in (55) are

$$\kappa_1 = -\frac{P_{NN}^{-1}\bar{\rho}\bar{c}^2}{\sqrt{\gamma}}, \quad \kappa_2 = -\frac{P_{NN}^{-1}\bar{\rho}\bar{c}^2\sqrt{(\gamma-1)}}{\sqrt{\gamma}}, \quad \kappa_3 = \frac{1}{m\sqrt{\gamma}}, \quad \kappa_4 = \frac{\sqrt{(\gamma-1)}}{m\sqrt{\gamma}}. \quad (56)$$

A.2 The non-linear scheme

The discrete version of the non-linear flow equation is written as

$$(1 + V_1)U_t = -\tilde{A}U + V_2\tilde{B}U + \tilde{\Sigma}(U - g(V)) + \tilde{\Pi}(U - r) \quad (57)$$

where \tilde{A} , $\tilde{\Sigma}$ and $\tilde{\Pi}$ are defined above and $\tilde{B} = (\Xi P^{-1}Q + P^{-1}Q\Xi - I_N) \otimes I_3/2$. The corresponding system to (51) and (52) in the nonlinear case becomes

$$(1 + V_1)U_t = (-\tilde{A} + \tilde{B} + \tilde{\Sigma} + \tilde{\Pi})U - \tilde{\Sigma}g - \tilde{\Pi}r \quad (58)$$

$$V_t = -BV + F. \quad (59)$$

The definitions of all the terms in (58) and (59) can be found in section A.1 above. The non-linear coupled equations formulated as a single system corresponding to (55) is

$$y_t = \begin{bmatrix} & & 0 & 0 \\ & & \vdots & \\ -\tilde{A} + \tilde{\Sigma} + \tilde{\Pi} + V_2\tilde{B} & & \vdots & \kappa_1 \\ & & 0 & \kappa_2 \\ 0 & \dots & 0 & 0 \\ 0 & \dots & 0 & 0 \end{bmatrix} \frac{y}{1 + V_1} + \begin{bmatrix} & & 0 & 0 \\ & & \vdots & \vdots \\ 0 & \dots & 0 & -B \\ 0 & \dots & \kappa_3 & 0 \end{bmatrix} y - \begin{bmatrix} \frac{\tilde{\Pi}r}{1 + V_1} \\ 0 \\ 0 \end{bmatrix} \quad (60)$$

where the coupling terms in (60) are the same as the ones in (55) and given by (56).

Acknowledgements

We thank Dr. Arnaud Malan at the Computational Aerodynamics Branch, Division of Defense, Peace, Safety and Security, CSIR South Africa for the support for this work.

References

- [1] J. Alonso and A. Jameson. Fully-implicit time-marching aeroelastic solutions. In *32th Aerospace Sciences Meeting*, number AIAA Paper 94-0056, Reno, January 1994.
- [2] K.J. Bathe, C. Nitikitpaiboon, and X. Wang. A mixed displacement-based finite element formulation for acoustic fluid-structure interaction. *Computers and Structures*, 56(2-3):225–237, 1995.
- [3] P. Geuzaine C. Farhat and G. Brown. Application of a three-field nonlinear fluid-structure formulation to the prediction of the aeroelastic parameters of an f-16 fighter. *Computers and Fluids*, 32:3–29, 2003.
- [4] M.H. Carpenter, J. Nordström, and D. Gottlieb. A stable and conservative interface treatment of arbitrary spatial accuracy. *Journal of Computational Physics*, 148:341–36, 1999.
- [5] M. Dalenbring and A. Zdunek. On the use of three-dimensional h- and p-version finite elements in solving vibration response problems. *Journal of Sound and Vibration*, 288(4-5):907–929, 2005.
- [6] E.H. Dowell and D. Tang. Nonlinear aeroelasticity and unsteady aerodynamics. *AIAA Journal*, 40(9):1697–1707, September 2002.
- [7] J.F. Gerbeau and M. Vidrascu. A quasi-newton algorithm based on a reduced model for fluid-structure interaction problems in blood flows. *Mathematical Modelling and Numerical Analysis*, 37(4):631–647, 2003.
- [8] C.J. Greenshields and H.G. Weller. A unified formulation for continuum mechanics applied to fluid-structure interaction in flexible tubes. *International Journal for Numerical Methods in Engineering*, 64:1575–1593, 2005.
- [9] Kreiss H.-O. Gustafsson, B. and Oliger. *Time-dependent problems and difference methods*. J. John Wiley and Sons, 1995.
- [10] J. De Hart, GWM Peters, PJG Schreurs, and FPT Baaijens. A three-dimensional computational analysis of fluid-structure interaction in the aortic valve. *Journal of Biomechanics*, 36(1):103–112, 2003.
- [11] H.-O. Kreiss and G. Scherer. *Finite element and finite difference methods for hyperbolic partial differential equations*, in: C. De Boor (Ed.), *Mathematical Aspects*

- of Finite Elements in Partial Differential Equation*. Academic Press, New York, 1974.
- [12] E. Di Martino, G. Guadagni, A. Funaro, and G. Ballerini. Fluid-structure interaction within realistic three-dimensional models of the aneurysmatic aorta as a guidance to assess the risk of rupture of the aneurysm. *Medical Engineering and Physics*, 23(9):647–655, 2001.
- [13] K. Mattsson. Boundary procedures for summation-by-parts operators. *Journal of Scientific Computing*, 18(1):133–153, 2003.
- [14] K. Mattsson and J. Nordström. Summation by parts operators for finite difference approximations of second derivatives. *Journal of Computational Physics*, 199:503–540, 2004.
- [15] J. Nordström. The use of characteristic boundary conditions for the Navier-Stokes equations. *Computers & Fluids*, 24(5), 1995.
- [16] J. Nordström. Conservative finite difference approximations, variable coefficients, energy estimates and artificial dissipation. *Journal of Scientific Computing*, 29:375–404, 2006.
- [17] J. Nordström and M. H. Carpenter. Boundary and interface conditions for high order finite difference methods applied to the Euler and Navier-Stokes equations. *Journal of Computational Physics*, 148:621–645, 1999.
- [18] J. Nordström and M. H. Carpenter. High-order finite difference methods, multidimensional linear problems and curvilinear coordinates. *Journal of Computational Physics*, 173:149–174, 2001.
- [19] B. Strand. Summation by parts for finite difference approximation for d/dx . *Journal of Computational Physics*, 110(1):47–67, 1994.
- [20] X. Wang and K.J. Bathe. Displacement/pressure based mixed finite element formulations for acoustic fluid-structure interaction problems. *International Journal for Numerical Methods in Engineering*, 40(11):2001–2017, 1998.